GA–A26433

CALCULATED BEAM PROFILES FOR THE DIII-D OFF-AXIS AND LONG PULSE NEUTRAL BEAM UPGRADE

by
H.K. CHIU, R.M. HONG and J.T. SCOVILLE

JUNE 2009

GENERAL ATOMICS

DISCLAIMER

This report was prepared as an account of work sponsored by an agency of the United States Government. Neither the United States Government nor any agency thereof, nor any of their employees, makes any warranty, express or implied, or assumes any legal liability or responsibility for the accuracy, completeness, or usefulness of any information, apparatus, product, or process disclosed, or represents that its use would not infringe privately owned rights. Reference herein to any specific commercial product, process, or service by trade name, trademark, manufacturer, or otherwise, does not necessarily constitute or imply its endorsement, recommendation, or favoring by the United States Government or any agency thereof. The views and opinions of authors expressed herein do not necessarily state or reflect those of the United States Government or any agency thereof.

GA–A26433

CALCULATED BEAM PROFILES FOR THE DIII-D OFF-AXIS AND LONG PULSE NEUTRAL BEAM UPGRADE

by
H.K. CHIU, R.M. HONG and J.T. SCOVILLE

This is a preprint of a paper to be presented at the 36th Symposium on Fusion Engineering, May 31 through June 5, 2009 in San Diego, California and to be published in the Proceedings.

Work supported by
the U.S. Department of Energy
under DE-FC02-04ER54698

GENERAL ATOMICS PROJECT 30200
JUNE 2009

GENERAL ATOMICS

Calculated Beam Profiles for the DIII-D Off-Axis and Long Pulse Neutral Beam Upgrade

H.K. Chiu, R.M. Hong and J.T. Scoville
General Atomics
P.O. Box 85608
San Diego, California 92186-5608 USA
chiuhk@fusion.gat.com

***Abstract*—An analysis of the propagation of a neutral beam along the axis of injection was performed. An analytic solution was found using a population of Gaussian point sources uniformly distributed on a surface in Cartesian coordinates normal to the direction of beam travel. The solution was extended to examine the effects of multiple source surfaces, incorporating the canting of the source surfaces that enables focusing the neutral beam. The model was then used to analyze the current DIII-D neutral beam ion sources (with an initial beam size of 12 x 48 cm) to obtain the beam profiles and intensities at locations downstream of the source plane. The calculated intensity profiles along the axis of beam travel lead to estimates of the scrape-off beam power loss to the beamline internal components. These results were compared to previous water-flow-calorimetry measurements of beam power depositions on the beamline internal components to validate the model. The model was then employed to calculate the beam profiles and beam intensities for the smaller aperture ion sources (12 x 43 cm) planned for use on the off-axis beamline. The calculated data are used in the mechanical and thermal analyses for the design of the internal components for the future off-axis beamline. The off-axis beamline will be capable of operating at 80 keV beam energy for pulse lengths up to 10 seconds. We present a description of the analysis methodology, the calculated and measured power deposition results, and a discussion of the implications and limitations of the analysis.**

Keywords: neutral beam, DIII-D

I. Introduction

It is useful to have an analytic model of beam propagation for a rectilinear source to predict beam power deposition to the internal components of a beamline when designing an upgrade. The various components of a DIII-D neutral beamline are highlighted in Fig. 1. The ion source was modeled as a set of Gaussian beamlets on planes at the entrance to the beamline. The treatment of beam power scrape-off on successive collimators, a definition for beam expansion to account for canted beam sources and a beam-into-gas energy loss model were developed to calculate expected beam power deposition along the beamline. Using the beam profiles generated with the Gaussian model for four 12 x 12 cm planar sources and the beam power loss algorithms, the DIII-D neutral beam intensity profile propagation and scrape-off power were modeled. The results were compared to the power deposition data measured with water flow calorimetry (WFC) on the existing DIII-D beamline internal components for validation.

II. The Gaussian Model

Consider the propagation of a Gaussian point source, centered on the origin traveling down the z-axis of a Cartesian system (see Fig. 2). The general solution for beam intensity at any point in the coordinate space is given by:

$$I(x,y,z) = I_0 \exp\left(-\mu_x^2\right)\exp\left(-\mu_y^2\right) \quad . \qquad (1)$$

Where $\mu_x = (x - x_0)/\alpha$ and $\mu_y = (y - y_0)/\beta$, the point (x_0, y_0) is the center of the Gaussian point source on the source plane, and (x, y) are the coordinates of a point on the target plane defined by $z = Z$.

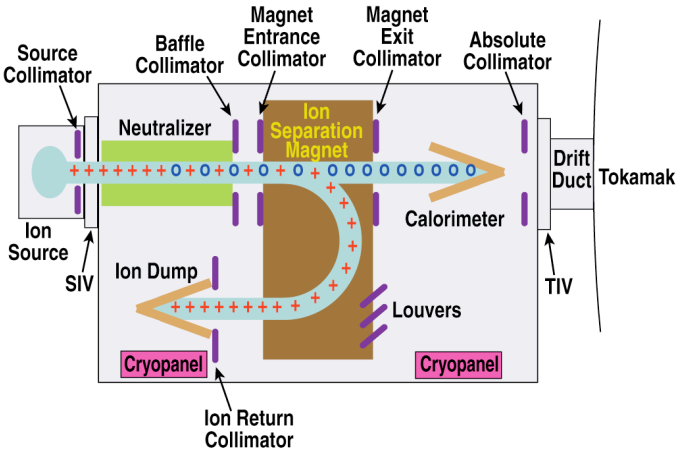

Figure 1. DIII-D Beamline internal components.

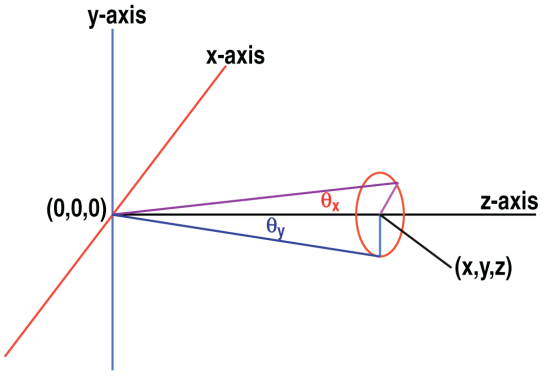

Figure 2. Gaussian point source in Cartesian system.

Equation (1) is an example of a normal distribution; the full width half maximum (FWHM) illustrated in Fig. 2 is related to the standard deviation of the normal distribution in the following manner:

$$\mathrm{FWHM}_x = 2Z\tan\theta_x = 2\sigma_x\sqrt{2\ln 2} \text{ and}$$
$$\mathrm{FWHM}_y = 2Z\tan\theta_y = 2\sigma_y\sqrt{2\ln 2} \quad ,$$

where σ_x is the standard deviation in the x-direction and σ_y is the standard deviation in the y-direction. This defines the beamlet divergence in the x-direction, α, and the beamlet divergence in the y-direction, β as $\alpha = \sigma_x\sqrt{2}$ and $\beta = \sigma_y\sqrt{2}$.

A planar source of width $2X_0$ and height $2Y_0$ composed of uniformly distributed Gaussian beamlets is shown in Fig. 3. The normalized beam intensity at any point on the $z = Z$ plane is given by integrating (1) over the planar source, bounded by $(\pm X_0)$ in the x-direction and $(\pm Y_0)$ in the y-direction on the source plane and dividing the result by the area of the source, resulting in an expression for normalized beam intensity at any point (x,y) on the target plane z, as a sum of error functions:

$$I(x,y,z) = \int_{-Xo}^{Xo}\int_{-Yo}^{Yo} I(x,y,z) = I_0\exp\left(-\mu_x^2\right)\exp\left(-\mu_y^2\right)$$
$$= \left(\frac{1}{16X_0Y_0}\right)\left\{erf\left(\frac{x-X_0}{\alpha}\right) - erf\left(\frac{x+X_0}{\alpha}\right)\right\}$$
$$\left\{erf\left(\frac{y-Y_0}{\beta}\right) - erf\left(\frac{y+Y_0}{\beta}\right)\right\} \quad , \qquad (2)$$

Integrating (2) over the target plane yields unity, i.e.: $\iint \mathrm{Eq.}\,(2) = 1$.

The case of interest in DIII-D is an ion source composed of three planar source modules. As illustrated in Fig. 4, the top and bottom planes are angled to focus the total beam at the canted module aim point (CMAP) down the axis of propagation. The contribution from the angled source modules can be brought into the coordinate system of the central plane by a simple transformation based on the distance to the CMAP and the angle between the angled modules' geometric normal and the axis of beam propagation. The expression for coordinate transformation of the canted source planes into the coordinate system defined by the axis of travel is given by:

$$y = y_1 - (\mathrm{CMAP} - z)\tan\phi$$
$$y = y_2 - (\mathrm{CMAP} - z)\tan\gamma \quad , \qquad (3)$$

where y_1 is the local vertical coordinate of the upper canted module, and y_2 is the local vertical coordinate of the lower canted module, and $\phi = \gamma$ for the DIII-D ion sources (top and bottom modules are tilted inward at equal angles).

Using the coordinate transformations given in (3) and summing (2) to account for three source modules, the normalized beam intensity for any point of interest on the target plane is found to be a sum of error functions. The general form of the equation for normalized neutral beam propagation in DIII-D is given by:

$$I_{tot}(x,y,z) = \left\{erf\left(\frac{x-X_0}{\alpha}\right) - erf\left(\frac{x+X_0}{\alpha}\right)\right\}$$
$$\left\{\begin{array}{l}\left(\frac{A_1}{16X_0Y_0A_{tot}}\right)\left\{erf\left(\frac{y-Y_0+CMAP}{\beta}\right) - erf\left(\frac{y+Y_0+CMAP}{\beta}\right)\right\} \\ +\left(\frac{A_2}{32X_0Y_0A_{tot}}\right)\left\{erf\left(\frac{y-Y_0}{\beta}\right) - erf\left(\frac{y+Y_0}{\beta}\right)\right\} \\ +\left(\frac{A_3}{16X_0Y_0A_{tot}}\right)\left\{erf\left(\frac{y-Y_0-CMAP}{\beta}\right) - erf\left(\frac{y+Y_0-CMAP}{\beta}\right)\right\}\end{array}\right\} \qquad (4)$$

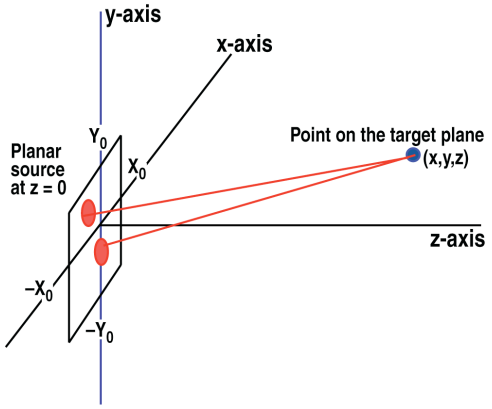

Figure 3. Beam intensity contributions at point (x,y,z) from 2 random Gaussian point sources on the source plane

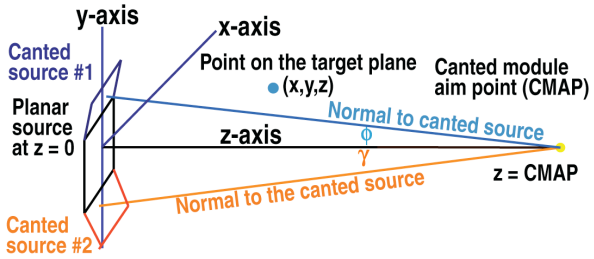

Figure 4. DIII-D neutral beam source model consisting of a central module and two canted modules.

An EXCEL spreadsheet encapsulating (4) was created to generate normalized beam intensity profiles for a typical DIII-D neutral beam comprised of four 12 x 12 cm rectilinear grid modules stacked into a 12 x 48 cm vertical array with the outer modules canted inwards at 1.083° for focusing (CMAP = 951 cm). Each angled module is treated explicitly while the two central non-angled modules are represented in the model as a 12 x 24 cm module. A normalized beam intensity profile is converted to a beam energy profile by multiplying it by the total beam energy. The calculated DIII-D first quadrant (upper right quarter) normalized beam intensity profiles at the source collimator (z = 30 cm) and at the entrance to the calorimeter beam dump (z = 358 cm) are presented in Figs. 5 and 6. The beam intensity over the target plane is grouped into bands of width $2\times10^{-6}/\mathrm{mm}^2$, the outer bounding surface is the $1\times10^{-6}/\mathrm{mm}^2$ band, and represented in these figures by the transition between the outer purple and blue areas. Multiplying by the total beam energy converts the normalized intensity bands into beam energy density bands (kJ/unit area).

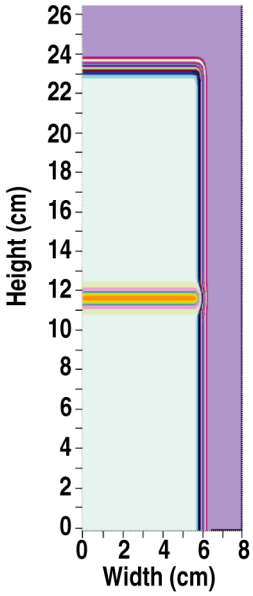

Figure 5. First quadrant of the intensity profile at the source collimator (z = 30 cm).

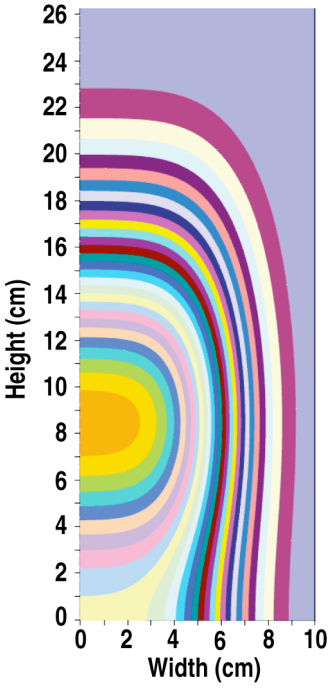

Figure 6. First quadrant of the intensity profile at the calorimeter entrance (z = 358 cm).

The peak intensity region (bounded by $3.8\times10^{-5}/\mathrm{mm}^2$ to $4\times10^{-5}/\mathrm{mm}^2$) is represented in orange in Figs. 5 and 6, and is located where beam from the outer angled module intersects the beam generated from the central source module. The peak intensity band moves closer to the center of the plot as the target surface moves toward the CMAP.

We define the edge of the beam as the bounding surface that contains 99.5% of the beam energy. The expansion of the beam profile in the vertical direction can be mapped by noting the intersection of the bounding surface to the $y-z$ plane at various values of z. Likewise the horizontal beam expansion was mapped by noting the intersection of the bounding surface to the $x-z$ plane at various values of z.

Fig. 7 illustrates the process for determining the beam expansion in the vertical (y) direction. The line $y(z) = y(0) + az$ traces the growth of the bounding surface in the y direction. The value $y(0)$ corresponds to the y-value of the bounding surface at $z = 0$, the constant a, is the vertical expansion factor. Fig. 7 also illustrates the scrape off process; y_n and y_{n-1} are collimator aperture half-heights at positions z_n and z_{n-1}. Beam particles that pass the collimator at z_{n-1} are assume to expand past the collimator by the beam expansion factor a, to the next collimator at z_n, and intercept that collimator between y_n and $y_{n'}$. Beam particles between y_n and $y_{n'}$ will be loss to collimator n.

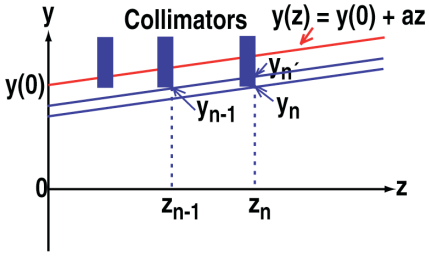

Figure 7. Simple beam scrape-off model.

III. Model Validation

Using the scrape-off method, the beam interception area for each collimator was found. The beam intensities that shine onto each interception area are converted into energy absorbed by each collimator. Table I shows the percentage of the initial energy from the source absorbed by each collimator as calculated by the simple scrape-off method compared to that measured by WFC.

TABLE I. Comparison of the Percentage of Initial Source Energy Deposited for Several Beamlet Divergences with WFC Data

Beamline Component	Total Calculated Energy Deposited on Component {0.4°,0.8°} (%)	Total Calculated Energy Deposited on Component {0.6°,1.2°} (%)	Total Calculated Energy Deposited on Component {0.7°,1.4°} (%)	Deposited Energy Measured by WFC (%)
Source collimator	1.47	1.96	2.43	3.20
Neutralizer body	1.20	3.08	4.37	4.50
Baffle	0.08	0.21	0.33	1.40
Magnet entrance	0.28	0.8	0.90	1.00
Magnet exit	1.00	0.96	1.89	1.90
Calorimeter	95.95	92.95	90.60	86.90

Preliminary beamlet divergence angles of $\alpha = 0.4°$ and $\beta = 0.8°$ were calculated based on the measured FWHM of the beam at the calorimeter with an array of 42 thermocouples

embedded in the calorimeter, assuming a purely Gaussian profile. However, the canting of the upper and lower modules of the DIII-D neutral beam ion sources results in a double-peak profile at the calorimeter, suggesting that the beamlet divergence chosen may not be appropriate. The ion sources were designed by the Lawrence Berkeley Laboratory [1] to have beamlet divergences of $\alpha = 0.6°$ and $\beta = 1.2°$. The scrape-off energies arising from these design value divergences, the divergence values calculated by the calorimeter, and those for a poorer optics case are shown in Table I.

In all cases considered, the energy deposition measured by WFC is higher than the calculated scrape-off energies on the collimators, although the calculated values for the poorer optics cases are considerably closer to the WFC measurements. However, the Gaussian beam calculation does not account for energy loss of beam particles slowing down in the background neutral gas and the resultant scattering of the neutral gas onto the collimators. The background neutral gas is present in the beamline from the gas supply of the ion source and from the neutral gas input to the neutralizer cell.

A first order estimate using stopping power data was made of the possible energy loss from beam ions slowing down in the neutral background gas in the neutralizer cell and baffle area of the beamline. The stopping power data [2] for D^+ slowing down in D_2 is given in Fig. 8. Given an average peak gas puff rate of 8 torr-l/s neutral gas into the neutralizer, a neutralizer volume of 8.68×10^4 cm^3 and a path length of 113 cm. A beam energy loss of ~ 5.4% was calculated for a 80 keV beam. The energy lost to the neutral gas background will be deposited on the components nearest the neutralizer, such as the neutralizer, baffle collimator and magnet entrance collimator. These losses will also reduce energy directed to the calorimeter, suggesting a redistribution of beam energy that is consistent with the energy loss variances found between the Gaussian model and the WFC data.

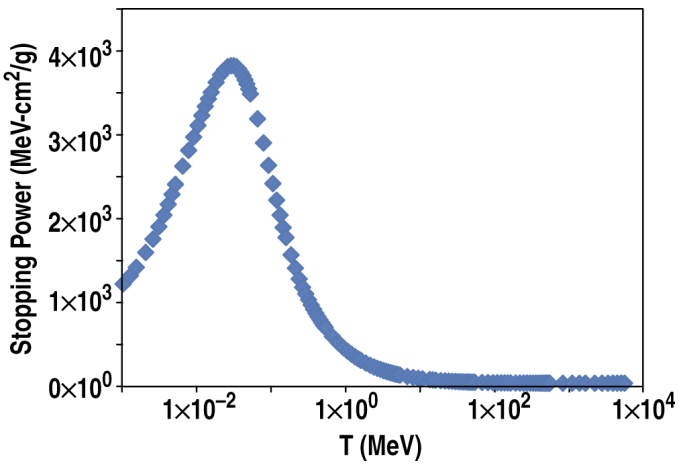

Figure 8. Stopping power data for D^+ in D_2.

IV. Summary and Discussion

An analytic model for Gaussian beam propagation was derived for the DIII-D neutral beam. The model was used to generate beam intensity profiles at locations corresponding to the collimator positions in the DIII-D beamlines. The scrape-off energy on these collimator surfaces were calculated from the beam intensity profile interception area. The calculated scrape-off energy was compared to the energy deposition on these components measured with WFC. Significant variance between the calculated scrape-off and the measured data was observed. Although calculations with larger beamlet divergences (poorer beam optics) agrees better with the measured WFC data, it was recognized that scrape-off is not the only mechanism for beam energy loss to the beamline components. A first order calculation was made of the beam energy loss to the background neutral gas in the neutralizer cell by using the stopping power data for energetic D^+ slowing down in a D_2 background.

It is clear that beam energy loss cannot be completely predicted by using a Gaussian beam propagation model alone. However, it is possible to define the area of beam interception on the various collimators by projecting the Gaussian beam intensity profile onto those collimators and using the simple scrape-off model. By using the calculated beam interception area on a component and the corresponding beam energy deposition measured by WFC to that component, a conservative heat loading value was derived for the components of interest. These conservative heat loading values are then used in the design of the beamline internal components for the future off-axis and long pulse beam upgrade.

Future work is planned to try to resolve the discrepancy between the Gaussian model and the measured energy deposition. The charge exchange recombination (CER) system utilizes several of the DIII-D beams and monitors the Doppler shift of the D_α light from beam particle interactions in the plasma. Analyses of the CER data, for a range of neutralizer gas puff rates (0 to 15 torr-l/s) is planned. From the analyses, we can determine if a shift in the observed D_α wavelength occurs, and if such a shift is seen, then the corresponding energy loss of the beam due to the neutralizer gas may help to reconcile the discrepancies between the calculated energy scrape-off and the WFC data.

Acknowledgment

This work supported by the U.S. Department of Energy under DE-FC02-04ER54698.

References

[1] W. Lindquist and S. Staten "Evolution of the Common Long Pulse Neutral Beam Source Program" Proc. 12th Symp. on Fusion Engineering, October 1987, p 1130.

[2] M.J. Berger, J.S. Coursey, M.A. Zucker and J. Chang "Stopping-Power and Range Tables for Electrons, Protons, and Helium Ions" National Institute of Standards and Technology, PSTAR database, August 2005.